# The Influence of Precipitation on the Work-Hardening Behavior of the Aluminum Alloys AA6111 and AA7030

L.M. CHENG, W.J. POOLE, J.D. EMBURY, and D.J. LLOYD

Tensile tests were conducted on the aluminum alloy, AA6111, after various artificial aging treatments in order to examine the influence of precipitation state on yield stress and work-hardening behavior. During artificial aging, significant changes in the work-hardening rate were observed as the precipitation reaction proceeded. A semiempirical model has been developed to interpret these changes in work-hardening rate. This model shows that the significant changes in work-hardening rate can be related to the manner in which flow stress contributions from different obstacles are summed and the transition from shearable to nonshearable precipitates. The present study presents a new approach to determining the shearable/nonshearable transition from a series of tensile tests. Results on the aluminum alloy AA7030 were also found to be consistent with the proposed theoretical framework. Finally, the proposed model allows the overall mechanical response for a variety of aging conditions to be rationalized.

## I. INTRODUCTION

OVER the past decades, two important problems in plasticity—namely, the accumulation of dislocations during the plastic flow of a single-phase material and the interaction of dislocations and second-phase particles, have received much attention.[1–7] Comprehensive models and careful experimental verification exist for both these problems. A basic framework for work hardening has been established,[4,5,6] which considers the hardening process as a competition between dislocation accumulation and the loss of dislocation line length (*i.e.,* dynamic recovery). However, when a complex problem such as the optimization of the heat treatment for precipitation hardening Al alloys in order to provide maximum formability is considered, the available theoretical descriptions are less secure. The complexity arises because precipitates and their related solute distribution can influence the accumulation of dislocations in three distinct ways: (a) by influencing the mean free path of dislocations, (b) by creating an additional dislocation storage mechanism due to the compatibility of flow needed if the particles are hard and impenetrable, and (c) by influencing the rate of dynamic recovery.

The addition of alloying elements to form solid solutions is known to modify the work-hardening behavior,[8,9] primarily by making dynamic recovery a more difficult process.[10] This may arise from multiple mechanisms, *i.e.,* changes in stacking fault energy due to alloying, solute drag effects on dislocations,[2,3] *etc.* For materials containing precipitates, further complications arise. The work-hardening behavior of precipitate-containing alloys can be significantly affected by the nature of precipitates. For example, Byrne *et al.*[11] examined the stress-strain behavior of single crystals in the Al-Cu system. These authors observed a large difference in work-hardening behavior for samples with shearable and nonshearable precipitates. This was due to the observation that for samples with nonshearable precipitates, the single crystals immediately began deformation by polyslip rather than single slip and as a result no easy glide region was observed. However, in polycrystals where deformation begins with polyslip, the situation is less clear. Here, the effect of shearable precipitates on work hardening has generally been considered in terms of the possibility of flow localization on the glide plane[12] as the precipitate strength is decreased by the dislocation shearing process. On the other hand, for the case where a low volume fraction of nonshearable particles is present, very high initial hardening rates are observed (*i.e.,* dispersion hardening systems). This has been attributed to two fundamental mechanisms, *i.e.,* the storage of additional so-called geometrically necessary dislocations[2,13] or the storage of elastic energy in the second-phase particles.[14] Either of these viewpoints leads to large initial hardening rates and a large change in the overall work-hardening characteristics.[15] Finally, for materials with multiple sets of obstacles (*e.g.,* forest dislocations, solute atoms, and precipitates), careful consideration must be given to the appropriate method for adding the flow stress contributions to determine the yield stress.[16–19] As the density of forest dislocation increases during deformation, additional complications for the addition of flow stress contributions need to be considered to understand work-hardening behavior.[20]

Clearly, work hardening in precipitation-hardening systems is considerably more complicated than for high-purity materials or even solid solutions. However, it is of considerable interest to study this behavior in the more complex precipitation-hardening systems, since this may offer additional insight into the mechanisms of precipitation and work hardening. In addition, work-hardening behavior is of significant relevance to industrial processes such as metal

L.M. CHENG, formerly Postdoctoral Fellow, Department of Metals and Materials Engineering, The University of British Columbia, is with Defence R&D Canada, Atlantic Emerging Materials Section, Halifax, NS, Canada B3K 5X5. W.J. POOLE, Associate Professor, is with the Department of Metals and Materials Engineering, The University of British Columbia, Vancouver, BC, Canada V6T 1Z4. Contact e-mail: warren.poole@ubc.ca J.D. EMBURY, Professor, is with the Department of Materials Science and Engineering, McMaster University, Hamilton, ON, Canada L8S 4L7. D.J. LLOYD, Principal Scientist, is with the Kingston Research & Development Centre, Alcan International, Kingston, ON, Canada K7L 5L9.

Manuscript submitted February 12, 2002.

**Table I. Compositions of Alloys (Weight Percent)**

| Alloy | Zn | Mg | Si | Cu | Fe | Mn | Cr | Ti | Zr |
|---|---|---|---|---|---|---|---|---|---|
| AA6111 | — | 0.8 | 0.6 | 0.7 | 0.25 | 0.2 | 0.05 | 0.06 | — |
| AA7030 | 5.6 | 1.25 | 0.5 | 0.3 | 0.14 | — | — | — | 0.03 |

forming. Thus, the objective of the present work is to develop a satisfactory understanding such that the flow stress and hardening rate can be rationalized as a function of plastic strain for a variety of precipitate distributions. This work provides a detailed experimental study on work-hardening behavior for the industrial alloy AA6111 and the development of an semiempirical model to help understand these results. The results will also be compared to data for AA7030.

## II. EXPERIMENTAL PROCEDURE

AA6111 aluminum alloy was obtained from Alcan International (Kingston, Ontario, Canada) in sheet form, 1 mm in thickness. The material had been industrially cold rolled and then processed through a continuous annealing line where the alloy was recrystallized and solution heat treated. Samples of the AA7030 aluminum alloy were received from Hydro-Raufoss (Raufoss, Norway) in the form of extruded plates. The chemical compositions of these two alloys are given in Table I.

In order to produce samples with different states of precipitation, AA6111 was first solution treated for 20 minutes in a salt bath at 560 °C, water quenched, and then artificially aged at 220 °C or 250 °C in an oil bath for different aging times. To obtain a high density of precipitates in the AA7030 aluminum alloy, multistep aging treatments, including natural aging and two-step artificial aging treatments, were used. The material was first solution treated for 20 minutes at 480 °C in an air furnace, followed by water quenching and then natural aging for 24 hours at room temperature. After natural aging, the samples were aged at 100 °C for 5 hours followed by aging at 180 °C for up to 7 days. It has been shown that for 7000 series aluminum alloys, natural aging prior to the subsequent artificial aging leads to a finer distribution of precipitates, which results in a higher peak strength.[21]

Tensile tests were conducted on these alloys at room temperature after different aging conditions at a nominal strain rate of $2 \times 10^{-3}$ $s^{-1}$ using a MTS (Eden Prairie, MN) servohydraulic system with an Instron (Canton, MA) 8500 controller. For all tests, deformation was measured in the reduced section of the specimens using an extensometer with a 25-mm gauge length. The work-hardening rate was determined by numerically differentiating the true stress–true strain data using a moving regression analysis. For each data point on the $\sigma$-$\varepsilon$ curve, it and the six adjacent data points were used to obtain a best-fit linear regression line. The slope of the linear regression line was then treated as the work-hardening rate at that point. The resulting derivative was then smoothed to reduce the noise in the data.

## III. RESULTS

The plastic portions of the stress-strain curves for AA6111 with different levels of aging are shown in Figures 1(a) and (b) for underaged and overaged samples. In Figure 1(a), it can be observed that the supersaturated solid solution (SSS) shows substantial evidence of serrated flow. This diminishes as aging proceeds with no evidence at the peak strength. There is only a small difference in the plastic stress-strain behavior between the SSS and underaged sample (*i.e.,* at approximately 1/3 of the peak strength). The most striking feature that can be observed from these data is the dramatic drop in the level of work hardening as aging proceeds from the underaged to peak-aged condition. Both the initial work-hardening rate and the magnitude of the flow stress increase at a given strain are dramatically reduced. One practical effect of this decrease in work-hardening capacity as the flow stress is increased is the drop in the uniform elongation of the peak-aged material. In contrast, Figure 1(b) shows data for overaged samples, where one observes an initially almost linear hardening rate, which is at a much

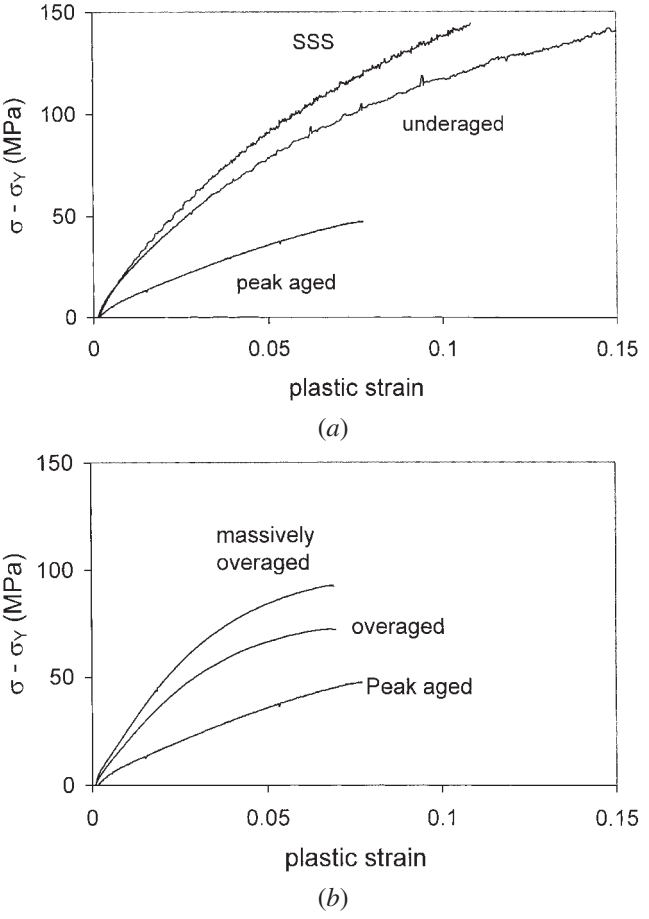


Fig. 1—(*a*) Plastic stress-strain curve for underaged and peak-aged curves; yield stress for supersaturated solid solution (SSS), underaged, and peak aged are 55, 150, and 335 MPa, respectively. This corresponds to an aging treatment of as solution treated, 1 min at 220 °C and 1 h at 220 °C, respectively. (*b*) Plastic stress strain curves for overaged samples. Yield stress for the peak-aged, overaged, and massively overaged are 335, 185, and 140 MPa, respectively. This corresponds to an ageing treatment of 1 h at 220 °C, 50 days at 220 °C, and 7 days at 250 °C, respectively.

higher level than the peak-aged condition followed by a distinctively rapid drop off in the level of work hardening at larger strains for the overaged samples.

It is conventional to examine work-hardening behavior by plotting the instantaneous work-hardening rate *vs* the flow stress increase (*i.e.,* $\sigma$-$\sigma_Y$). Figure 2 shows the data for a selected number of samples that have been aged at 220 °C. These data provide quantitative confirmation for the qualitative observations made regarding Figure 1. All curves show an initially very rapid decrease in the slope of the $\sigma$-$\varepsilon$ curve, which is associated with the elastic plastic transition. After the elastic/plastic transition, there are two distinctive types of behavior. For underaged and peak-aged samples, there is an approximately linear decrease of work-hardening rate as the flow stress increases. For the overaged samples, after the elastic/plastic transition, the work-hardening rate shows an almost constant hardening rate followed by a sharp decrease in hardening rate as the flow stress increases. Overall, the initial hardening rate first drops as aging proceeds (*e.g.,* for 1 minute and 1 hour at 220 °C) and then increases during overaging (49 hours and 50 days at 220 °C). In order to characterize these effects quantitatively, two operational parameters have been defined, as shown in Figure 3. The first parameter is $\theta_{max}$ and it is defined as the maximum work-hardening rate in the plastic regime. The second parameter is $d\theta/d\sigma$ and it is defined as the slope of the $\theta$-$\sigma$ plot. For the samples with a nonlinear $\theta$-$\sigma$ behavior, the slope is taken asymptotically as $\theta$ goes to zero.

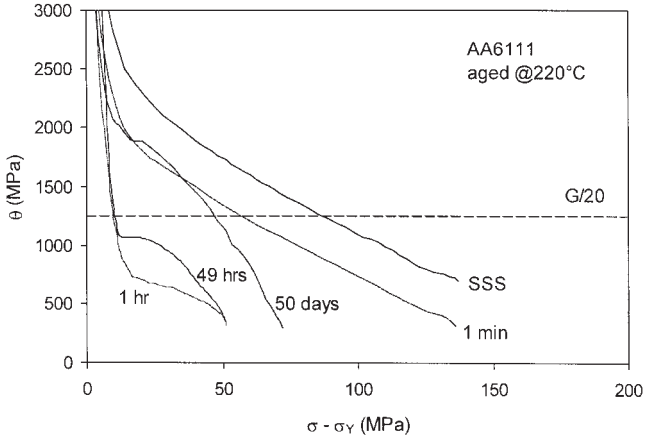


Fig. 2—The instantaneous work-hardening rate *vs* reduced flow stress for AA6111 samples aged at 220 °C.

The results for the analysis of the initial work-hardening rate as a function of the yield stress are shown in Figure 4. It can be observed that as the yield stress first increases during aging, the initial work-hardening rate decreases to a minimum near the peak strength. There is then a constant or slightly increasing value for $\theta_{max}$ as the yield stress drops during overaging. Once the overaged yield stress drops below approximately 275 MPa, $\theta_{max}$ dramatically increases. Figure 4(b) shows the evolution of $d\theta/d\sigma$ during aging. The value of $d\theta/d\sigma$ is almost constant up to the peak strength with a magnitude of 12.5 to 15. Again, at a yield stress of approximately 275 MPa, the magnitude of $d\theta/d\sigma$ increases dramatically and then remains constant at a value of 35 to 40.

In Section IV, the physical significance of these operational parameters will be examined and it will be shown that the dramatic change in the $\theta_{max}$ and $d\theta/d\sigma$ at an overaged yield stress of approximately 275 MPa is consistent with this being the shearable/nonshearable transition point.

## IV. DISCUSSION

The theoretical framework for the development of constitutive laws for alloys containing shearable and nonshearable precipitates has recently be reviewed by Estrin.[2] The formulism for the evolution of dislocation density with plastic strain can be written as a generalization of the Kocks/Mecking[4] approach; *i.e.,*

$$\frac{\partial \rho}{\partial \varepsilon^P} = (k_1 \rho^{1/2} - f k_2 \rho + k_D) \qquad [1]$$

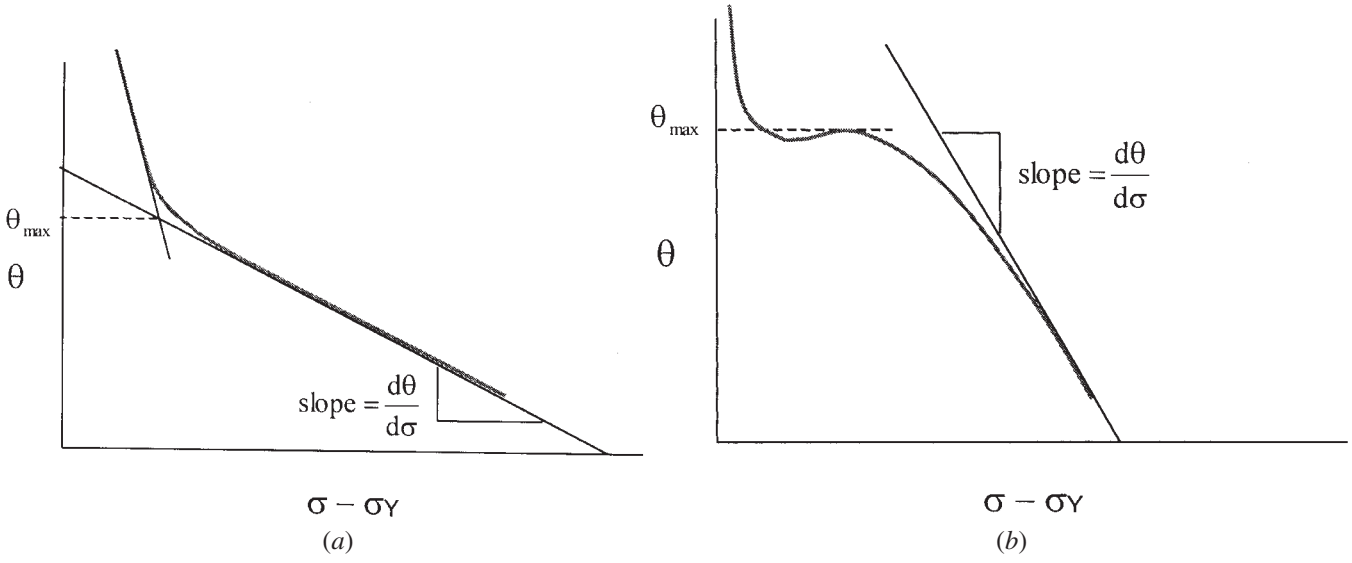


Fig. 3—Schematic diagram showing the definition of $\theta_{max}$ and the slope $d\theta/d\sigma$ for the two characteristic behaviors observed: (*a*) linear $\theta$-$\sigma$ and (*b*) nonlinear $\theta$-$\sigma$ plots.

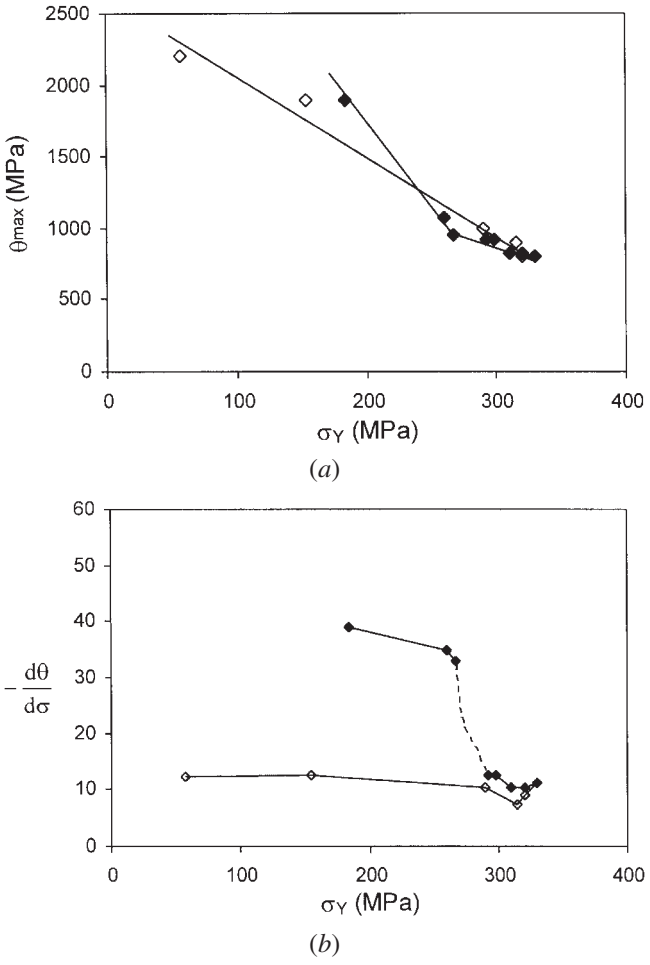


Fig. 4—Plots of the operational parameters *vs* yield stress for AA6111: (*a*) $\theta_{max}$ *vs* the yield stress and (*b*) the slope $d\theta/d\sigma$ *vs* the yield stress. Note: open symbols for underaged samples and closed symbols for overaged samples.

where $\rho$ is the dislocation density, $\varepsilon^P$ is the plastic strain, and $k_1$, $k_2$, $f$, and $k_D$ are constants. The first term on the right side of Eq. [1] represents the dislocation storage rate due to trapping of dislocations by other dislocations, and this is geometrically related to the mean free path of the dislocation. The second term is the dynamic recovery term, which is dependent on temperature, strain rate, and solute concentration, and $f$ represents a modifying factor due to the effect of dislocation/precipitate interactions on dynamic recovery. Finally, the last term is due to the storage of geometrically necessary dislocations due to nonshearable particles. The flow stress contribution from dislocation hardening, $\sigma_\perp$, can be written as

$$\sigma_\perp = \alpha_\perp G\mathbf{b}M\rho^{1/2} \qquad [2]$$

where $\alpha_\perp$ is a constant of order 0.3, **b** is the magnitude of the Burgers vector, $G$ is the shear modulus (25.4 GPa), $M$ is the Taylor factor (*i.e.,* 3.06 for fcc metals), and $\rho$ is the dislocation density. Furthermore, Estrin[2] suggests that the flow stress can be taken as a linear sum of the precipitation and dislocation-hardening contributions:

$$\sigma = \sigma_\perp + \sigma_{\text{ppt}} \qquad [3]$$

However, for situations where multiple sets of obstacles are present such as precipitates and dislocations, Kocks[20] has proposed that other superposition laws should be considered when examining work-hardening behavior. In the present work, it is proposed that a more general form for the flow stress addition law be taken to include the solid-solution-strengthening component and to account for different ways of summing the precipitation and dislocation hardening contributions; *i.e.,*

$$\sigma = \sigma_{ss} + (\sigma_\perp{}^n + \sigma_{\text{ppt}}{}^n)^{1/n} \qquad [4]$$

where $n$ can vary between 1 and 2, and $\sigma_{ss}$ is the contribution from the solid solution. The question of addition laws has received considerable attention[16,18,19] and has been related to relative density and strength of the obstacles to dislocation motion. This is of particular relevance to the present work since the strength of precipitates as obstacles increases as the precipitate size increases during aging. The limiting cases are as follows: The computer simulations of Foreman and Makin[16] suggest that the case of $n = 1$ only applies when there is a high density of weak obstacles and a low density of strong obstacles. This would correspond to the early stages of precipitation when there is a high density of weak precipitates and a low density of forest dislocations (strong obstacles). On the other hand, for later stages of aging, there is a condition where the obstacle strength of the precipitates and the average obstacle strength for cutting of forest dislocations would be identical. For this case, a value of $n = 2$ would be appropriate (*i.e.,* one should clearly add the obstacle densities not the flow stress contributions). At intermediate cases, the appropriate value of $n$ falls between these extremes. The implications of this on the work-hardening behavior will be considered in the following sections.

### A. *Shearable Precipitates—Effect of Flow Stress Addition Law*

In the case of shearable precipitates, the term $k_D$ in Eq. [1] is equal to zero; *i.e.,*

$$\frac{\partial\rho}{\partial\varepsilon^P} = (k_1\rho^{1/2} - f_s k_2\rho) \qquad [5]$$

where the term $f_s$ is a factor relating to the effect of shearable precipitates on dynamic recovery. Combined with Eq. [2], this may be directly integrated to give the well-known Voce equation:

$$\sigma_\perp = \sigma_{\perp s} - \sigma_{\perp s}\exp\left(-\frac{\theta_{\perp o}}{\sigma_{\perp s}}\varepsilon^P\right) \qquad [6]$$

where $\sigma_{\perp s}$ is the saturation stress for the dislocation hardening contribution and $\theta_{\perp o}$ is the initial work-hardening rate for dislocation contribution to flow stress. The constants $\sigma_{\perp s}$ and $\theta_{\perp o}$ can be directly related to the terms $k_1$ and $k_2$ in Eq. [5] as

$$\theta_{\perp o} = \frac{\alpha_\perp G\mathbf{b}Mk_1}{2} \qquad [7]$$

and

$$\sigma_{\perp s} = \frac{\alpha_\perp G\mathbf{b}Mk_1}{f_s k_2} \qquad [8]$$

Combining Eq. [6] with the flow stress addition law given by Eq. [4] allows for a complete description of the work-hardening behavior of alloys containing shearable precipitates.

In Section III, two operational parameters ($\theta_{max}$ and $d\theta/d\sigma$) were defined to characterize the work-hardening behavior. It is now possible to explore the physical significance of these parameters in the described theoretical framework. After substituting Eq. [6] into Eq. [4] and then differentiating with respect to strain, the overall work-hardening rate, $\theta$, is given by

$$\theta = \left[\left[\sigma_{ppt}^n + \sigma_\perp^n\right]^{\frac{1-n}{n}} \sigma_\perp^{n-1}\right] \cdot \theta_{\perp o}\left(1 - \frac{\sigma_\perp}{\sigma_{\perp s}}\right) \qquad [9]$$

and the derivative $d\theta/d\sigma$ is given by:

$$\frac{d\theta}{d\sigma} = \theta_{\perp o}\sigma_\perp^{n-1}\left[\sigma_{ppt}^n + \sigma_\perp^n\right]^{\frac{1-n}{n}} \cdot \left(\left[\frac{(1-n)\sigma_\perp^{n-1}}{\sigma_{ppt}^n + \sigma_\perp^n} + \frac{n-1}{\sigma_\perp}\right] - \frac{1}{\sigma_{\perp s}}\left[\frac{(1-n)\sigma_\perp^n}{\sigma_{ppt}^n + \sigma_\perp^n} + n\right]\right) \qquad [10]$$

For the case of $n = 1$, the operational parameter $\theta_{max}$ is equal to $\theta_{\perp o}$ in Eq. [9]. In this case, the term, $\theta_{max}$, has a clear physical basis as it is directly related to the dislocation storage term, $k_1$, through Eq. [7]. Also, for $n = 1$, the parameter, $d\theta/d\sigma$, reduces to

$$\frac{d\theta}{d\sigma} = -\frac{\theta_{\perp o}}{\sigma_{\perp s}} \qquad [11a]$$

or, by substituting Eqs. [7] and [8] into Eq. [11a],

$$\frac{d\theta}{d\sigma} = \frac{-f_s k_2}{2} \qquad [11b]$$

Therefore, $d\theta/d\sigma$ also has a clear physical basis; it is directly proportional to the rate of dynamic recovery, $k_2$.

However, for $1 < n < 2$, the overall initial work-hardening rate $\theta_{max}$ is given by

$$\theta_{max} = \left[\left[\sigma_{ppt}^n + \sigma_\perp^n\right]^{\frac{1-n}{n}} \sigma_\perp^{n-1}\right]\theta_{\perp o} \qquad [12]$$

The term $\left[\left[\sigma_{ppt}^n + \sigma_\perp^n\right]\right]^{\frac{1-n}{n}} \sigma_\perp^{n-1}\Big]$ is always less than unity and its magnitude is reduced as either the value of $n$ or $\sigma_{ppt}$ increases. In this case, the magnitude of $\theta_{max}$ loses its direct physical basis (it is no longer solely related to the dislocation storage term), but it can be clearly rationalized as a direct consequence of the incorporation of the addition law into the analysis, *i.e.*, the overall initial work-hardening rate is reduced, *viz.,* the work-hardening rate solely due to dislocation hardening for $1 < n < 2$.

On the other hand, when $1 < n < 2$, the second operational parameter, $d\theta/d\sigma$, has a complicated functional form given by Eq. [10]. However, it can be shown through a series of calculations that when $1 < n < 2$, and except for small values of $\sigma_{\perp s}$, reasonable combinations of $\sigma_{\perp s}$ and $\sigma_{ppt}$ give

$$\frac{d\theta}{d\sigma} \approx -\frac{\theta_{\perp o}}{\sigma_{\perp s}} \qquad [13]$$

Thus, this operational parameter is independent of the addition law and can still be physically related to the rate of dynamic recovery, $k_2$, through Eq. [11b].

### B. *Calculations—Shearable Precipitates: The effect of n*

To better illustrate the implications of this analysis, a series of calculations have been conducted. Reasonable values for $k_1$ and $k_2$ have been chosen by fitting to the experimentally determined stress-strain curve for the supersaturated solid solution curve ($k_1 = 7.5 \times 10^8$ m$^{-1}$, $k_2 = 27$, which correspond to values of $\sigma_{\perp s} = 185$ MPa and $\theta_{\perp o} = 2500$ MPa). Furthermore, to a first approximation, it is assumed that the geometric storage of dislocation line length is unaffected by shearable precipitates. On the other hand, the rate of dynamic recovery could decrease as the solid solution is depleted and precipitates are formed. These are competing processes as $k_2$ is proportional to solute content, which decreases during precipitation, while $f_s$ would be expected to increase when precipitates form. As a starting point, it will be assumed that these effects cancel each other out so that the product, $f_s k_2$, does not change, *i.e.*, $f_s = 1$.

The results of these calculations for different values of $n$ are shown in Figure 5. Comparison with the experimental results suggests that a good fit to the data at the peak strength can be found for a value of $n = 1.5$ to 2. Notice the dramatic drop in the initial work-hardening rate as the value of $n$ is increased. This compares favorably with Figure 4(a), which shows that as the yield stress of the alloy increases, the initial work-hardening rate dramatically decreases, reaching a minimum near the peak strength.

In addition, the data for the variation of $d\theta/d\sigma$ with yield stress shown in Figure 4(b) can now be interpreted as a direct measure of the rate of dynamic recovery. In Figure 4(b), it can be observed that the value of $d\theta/d\sigma$ is essentially a constant up to the peak strength. This is consistent with the

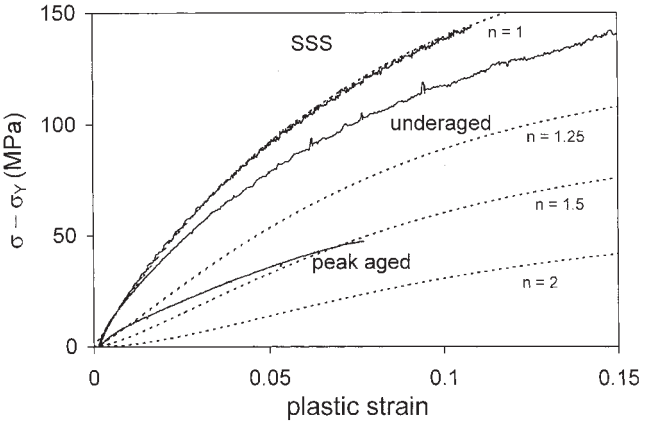


Fig. 5—Comparison of model calculations with experimental curves for different $n$ values assuming shearable precipitates with $\sigma_{ppt} = 300$ MPa, $k_1 = 7.5 \times 10^8$ m$^{-1}$, and $k_2 = 27$, which corresponds to values of $\sigma_{\perp s} = 185$ MPa and $\theta_{\perp o} = 2500$ MPa.

assumption that the rate of dynamic recovery does not significantly change when the precipitates are shearable. The experimentally determined value of $d\theta/d\sigma$ is about 12.5 to 15, which compares well with the value for $\frac{f_s k_2}{2} = 13.5$, which was used in the model calculations.

However, it is worth noting that at present there is only an empirical relationship between the appropriate value for $n$ and the yield stress of the alloy, *i.e.,* $n \to 2$ as $\sigma_Y$ increases. It is difficult to predict from first principals the nature of the addition law for the immediate cases where there is a mixture of obstacles with moderately different obstacle strengths. In these cases, it would be useful to have a more complete set of computer simulations similar to the work of Foreman and Makin.[16]

### C. *Nonshearable Precipitates*

It is expected that as the size of the precipitates increases, there will come a critical point when the dislocation will no longer shear the precipitate. Under these conditions, the deformation of the alloy is altered due to the storage of the so-called geometrically necessary dislocations around the nonshearable precipitates. As straining continues, it is expected that the initial array of Orowan loops will plastically relax by a variety of mechanisms such as the nucleation and glide of prismatic dislocation loops around the particles (Ashby[22] provides a more complete discussion). This process of storage and relaxation can be considered in an average sense, as an additional mechanism for storing dislocation line length, which is mathematically described by the term $k_D$ in Eq. [1].

In this work, it is assumed that the storage of dislocations is dominated by the mean free path between precipitates (this distance is much smaller than the average dislocation spacing) so that Eq. [1] reduces to

$$\frac{\partial \rho}{\partial \varepsilon^P} = (k_D - f_{ns}\, k_2\, \rho) \qquad [14]$$

Equation [14] can be directly integrated and combined with Eq. [2] to give

$$\sigma_\perp = \alpha G \mathbf{b} M \left[ \frac{k_D}{f_{ns} k_2} (1 - \exp(-f_{ns} k_2 \varepsilon^p)) \right]^{1/2} \qquad [15]$$

where $k_D$ is the storage term for geometrically necessary dislocations. It is assumed that nonshearable precipitates and forest dislocations are both strong obstacles. Therefore, the overall flow stress should be calculated by summing the obstacle densities on the glide plane (*i.e.,* $n = 2$). By combining Eqs. [2], [4], and [14], and then rearranging, the overall work-hardening rate can be shown to be given by

$$\theta = \left[ \frac{\sigma_\perp}{[\sigma_{\text{ppt}}^2 + \sigma_\perp^2]^{1/2}} \right] \cdot \left[ \frac{(\alpha G \mathbf{b} M)^2 k_D}{2\sigma_\perp} - \frac{f_{ns} k_2 \sigma_\perp}{2} \right] \qquad [16]$$

Differentiating Eq. [16],

$$\frac{d\theta}{d\sigma} = -\frac{(\alpha G \mathbf{b} M)^2\, k_D \sigma_\perp}{2\,(\sigma_{\text{ppt}}^2 + \sigma_\perp^2)^{3/2}} - \frac{f_{ns} k_2}{2} \left[ \frac{2\sigma_\perp}{(\sigma_{\text{ppt}}^2 + \sigma_\perp^2)^{1/2}} - \frac{\sigma_\perp^3}{(\sigma_{\text{ppt}}^2 + \sigma_\perp^2)^{3/2}} \right] \qquad [17]$$

Returning to the defined operational parameters used to characterize the work hardening in Section III, it can be seen that for small values of dislocation hardening, $\sigma_\perp$, the initial work-hardening rate, $\theta_{\max}$, is a function of $k_D/\sigma_{\text{ppt}}$. Since both $k_D$ and $\sigma_{\text{ppt}}$ are inversely proportional to the mean precipitate spacing, $\theta_{\max}$ becomes independent of the yield strength for overaging of nonshearable precipitates. This is consistent with the data shown in Figure 1(b), which show little change in the initial work-hardening rate when comparing the samples that are overaged and massively overaged. For the second operational parameter, recall that for overaged samples, where $\theta$ was not a linear function of the flow stress, the definition for $d\theta/d\sigma$ was chosen as $d\theta/d\sigma|_{\theta \approx 0}$.

Using this definition, it can be shown that Eq. [17] reduces to

$$\left.\frac{d\theta}{d\sigma}\right|_{\theta \approx 0} = -f_{ns}\, k_2 \qquad [18]$$

provided that $\sigma_\perp > \sigma_{\text{ppt}}$ (this is reasonable for overaged conditions where $\sigma_{\text{ppt}}$ is relatively small). Under these conditions, the operational parameter, $d\theta/d\sigma$, is again a direct measure of the rate of dynamic recovery, although this predicts that the magnitude of $d\theta/d\sigma$ is twice as large as for the case of shearable precipitates (*i.e*., compare to Equation [11b].

### D. *Calculations for Nonshearable Precipitates*

In order to conduct calculations, one must estimate values for $k_D$ and $f_{ns}\, k_2$. The geometric storage distance, $k_D$, is given by

$$k_D = \alpha_D \frac{M}{\mathbf{b} L} \qquad [19]$$

where $M$ is the Taylor factor, $\mathbf{b}$ is the magnitude of the Burgers vector, $L$ is the spacing of the precipitates on the glide plane,[22] and $\alpha_D$ is a constant. The spacing of obstacles can be calculated from the precipitation-hardening contribution:[23]

$$L = \frac{MF}{\mathbf{b}\sigma_{\text{ppt}}} \qquad [20]$$

assuming that for nonshearable precipitates, $F = 2T$, where $T$ is the line tension of the dislocation. A value of 0.3 for $\alpha_D$ was selected in order to have a reasonable fit to the initial rate of work hardening. The value of $f_{ns}\, k_2$ was chosen to be exactly the same value as was used in the calculations for shearable precipitates (*i.e.,* $f_{ns}\, k_2 = 27$). As shown in Figure 6, this choice of parameters gives reasonable agreement between the experiments and the model prediction. However, a close comparison with Figure 4b shows that the experimentally determined magnitude of $d\theta/d\sigma$ is 35-40, *i.e.*, approximately 1.3-1.5 times greater than that used in the model. Calculations have shown that increasing the magnitude of $f_{ns}\, k_2$ by this factor only has a minor effect on the predictions shown in Figure 6.

It does, however, suggest that the underlying rate of dynamic recovery is greater for the case of nonshearable precipitates than for solid solutions or shearable precipitates. This is not unreasonable since a cooperative mechanism for recovery of the relaxed structure can be envisioned. First, dislocations of opposite sign are locally stored around nonshearable precipitates. Recovery of these dislocations is relatively easy

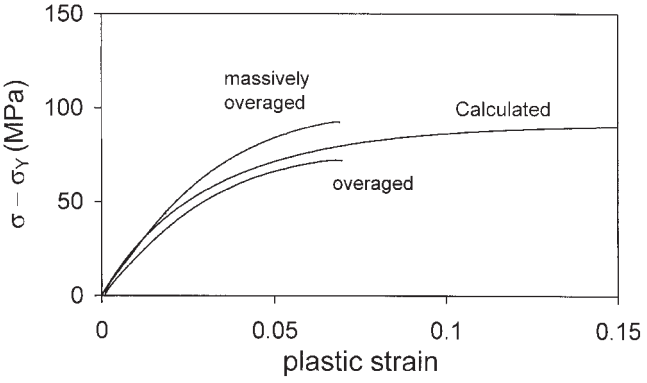


Fig. 6—Comparison of model calculations with experimental curves for overaged samples with nonshearable precipitates: $\sigma_{ppt}$ = 150 MPa, and $f_{ns}k_2$ = 27. Note: massively overaged and overaged correspond to 7 days at 250 °C and 50 days at 220 °C, respectively.

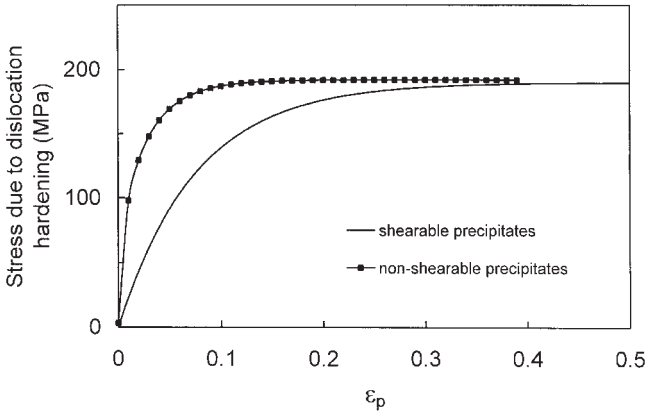


Fig. 7—Model calculations for dislocation hardening with shearable and nonshearable precipitates.

since the glide length for annihilation will be short. Second, for closely spaced nonshearable precipitates, the possibility exists for easy annihilation of oppositely signed loops from adjacent precipitates. These considerations can be used to rationalize the enhanced dynamic recovery rate that is experimentally observed under these conditions.

Experimentally, it is difficult to separate the dislocation hardening from the overall hardening behavior due to the effects of the flow stress addition law. However, it is possible to separate these effects using the model parameters. Figure 7 shows a comparison of the plastic stress-strain behavior due to dislocation hardening for the cases of shearable and nonshearable precipitates. The results are as expected, in the presence of nonshearable precipitates, the initial rate of dislocation hardening is much higher due to the extra storage of geometrically necessary dislocations. However, the saturation stress is very similar since this represents the physical limit to the density of dislocations that may be stored in the crystal.

### E. *Shearable/Nonshearable Transition Point*

It is not apparent *a priori* that the shearable/nonshearable transition should occur at the peak strength. Strengthening due to precipitation is given by

$$\sigma_{ppt} = \frac{MF}{\mathbf{b}L} \qquad [21]$$

The peak strength is given by the highest value of $F/L$, which may not be when $F$ is at its maximum (*i.e.,* when $F = 2T$). In fact, there is strong evidence from the *in-situ* TEM work of Vivas *et al.*[24] that for a similar alloy (*i.e.,* AA6056), the precipitates are shearable at the peak strength. Also, the recently developed yield stress model for AA6111 of Esmaeili *et al.* explicitly assumes that the shearable/nonshearable transition occurs at an overaged condition.[25] The proceeding analysis shows that as a natural consequence of the dislocation accumulation laws for shearable and nonshearable precipitates (*i.e.*, Equations [5] and [14], respectively), the slope of the $\theta$-$\sigma$ plot, $d\theta/d\sigma$ undergoes a step change in magnitude at the shearable/nonshearable transition (*i.e.*, compare Equations [11b] and [18]). Based on these considerations, it is proposed that the shearable/nonshearable transition can be determined from this very distinctive change in magnitude of $d\theta/d\sigma$. This can be directly observed by the transition point in a plot of $d\theta/d\sigma$ *vs* $\sigma_Y$ such as that shown in Figure 4. For AA6111, the experimental data in Figure 4 would suggest that shearable/nonshearable transition occurs at an overaged yield stress of approximately 275 MPa (note the peak strength was 335 MPa).

Until this point, the change in work-hardening behavior has been considered from a phenomelogical point of view. It is useful to consider the shearable/nonshearable transition in terms of the precipitation sequence for AA6111. The Al-Mg-Si-Cu system has a complex precipitation sequence and it has been suggested that the precipitation sequence is dependent on the chemistry of the alloy, particularly the Mg/Si ratio and the concentration of Cu.[26,27] Lloyd *et al.*[28] proposed that the precipitation sequence in the AA6111 can be presented as

$$\text{SSS} \rightarrow \text{clusters/GP zones} \rightarrow \beta'' + Q' \rightarrow \text{equilibrium } Q + \text{Mg}_2\text{Si}$$

The different precipitation states during the aging of the AA6111 at 180 °C have been examined by Perovic *et al.*[29] and Wang *et al.*[30] It has been observed that a high density of very fine $\beta''$ precipitates is predominant for underaged conditions; while at the peak strength, $\beta''$ and small density of $Q$ precipitates are observed. For the overaged materials, long lath-shaped $Q$ precipitates are dominant. If it is assumed that the state of precipitates in underaged, peak-aged, and overaged conditions is similar for aging at 220 °C, then the shearable/nonshearable transition appears to be associated with the transition from $\beta''$ to Q′ precipitates, which occurs during overaging.

### F. *Application of Analysis to AA7030*

To examine this approach for another aluminum alloy, tensile tests were conducted on the alloy AA7030 for a range of underaged and overaged conditions. Figure 8 shows the $\theta$-$\sigma$ plot derived from the tensile tests. The results are similar to AA6111, *i.e.,* (1) the initial hardening rate first decreases and then later increases as aging proceeds, and (2) there is a large difference in the magnitude of $d\theta/d\sigma$ between underaged and overaged samples. Figures 9(a) and (b) show the plots of $\theta_{max}$ and $d\theta/d\sigma$ as a function of the yield stress. The initial work-hardening rate, $\theta_{max}$, shows a

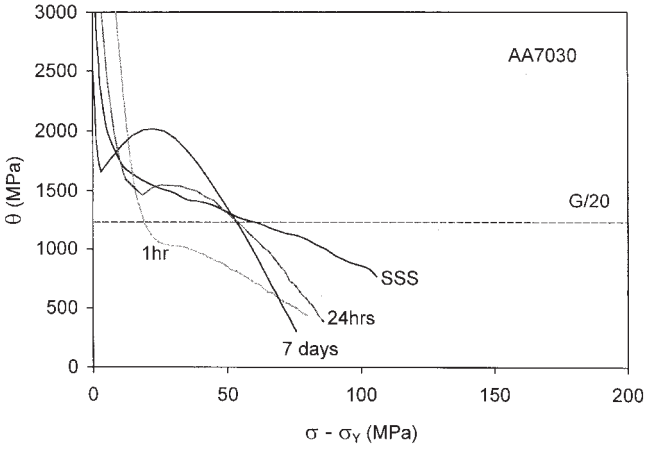


Fig. 8—The instantaneous work-hardening rate *vs* reduced flow stress for AA7030 samples aged at 180 °C.

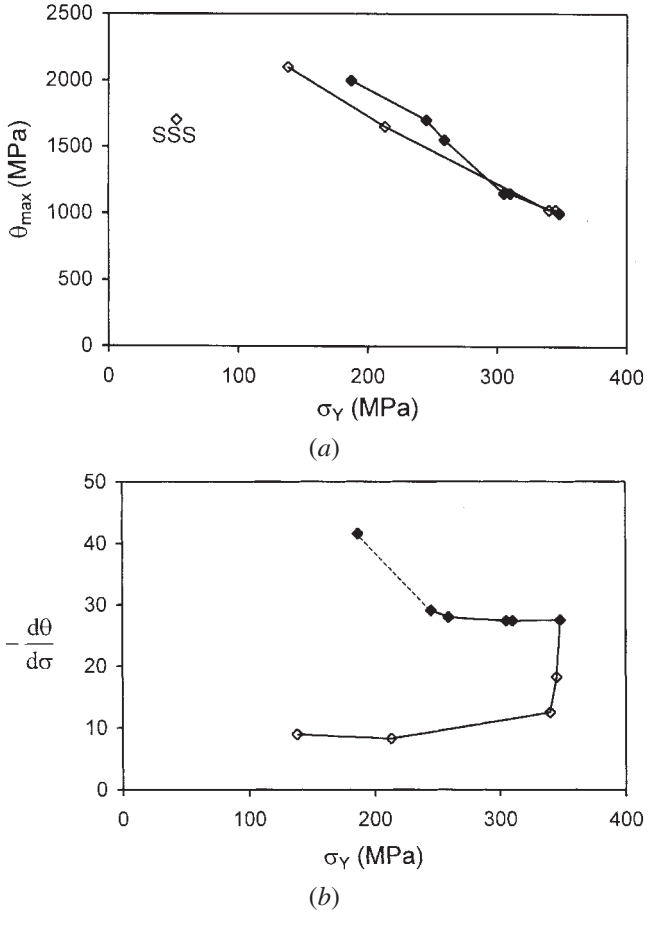


Fig. 9—Plots of the operational parameters *vs* yield stress for AA7030. (*a*) $\theta_{max}$ *vs* the yield stress and (*b*) the slope $d\theta/d\sigma$ *vs* the yield stress. Note: open symbols for underaged samples and closed symbols for overaged samples.

large drop as aging proceeds and reverses this trend very near to the peak strength. The parameter, $d\theta/d\sigma$, also shows a step change in behavior near the peak strength. In this case, it appears that the shearable/nonshearable transition occurs very near to the peak strength. This would be consistent with recent precipitation-hardening models by both Deschamps and Brechet[31] and Poole *et al.*,[32] which have assumed that the transition was at the peak strength for 7000 series alloys.

### G. *Application to Alloy Design*

Finally, it is worth commenting on the application of this work to the problem of alloy design in high-strength aluminum alloys. Near the peak strength, the overall ductility of these alloys is often limited by the necking, which occurs when the Considére condition is reached. In this work, we have shown that the work-hardening rate decreases as the peak strength is approached due to the nature of the flow stress superposition law. This is particularly important if the precipitates are shearable at the peak strength, since in this case, the underlying dislocation storage rate will be relatively low, resulting in the early formation of a neck. If, however, one could engineer the microstructure to have one set of particles to achieve strength (high density of small precipitates) and then add a second population of nonshearable particles to enhance the work-hardening contribution due to dislocation hardening, then it may be possible to delay necking. This idea is currently being examined from a theoretical and experimental point of view.

## V. CONCLUSIONS

A detailed experimental study of work-hardening behavior has been conducted for two commercial aluminum alloys, AA6111 and AA7030. Strong changes in work hardening were observed for different conditions of artificial aging. The analysis of the experimental results has focused on two parameters to characterize the work-hardening behaviour—the initial work-hardening rate, $\theta_{max}$, and the slope of the $\theta$-$\sigma$ plot, $d\theta/d\sigma$. The parameter $\theta_{max}$ is related to the initial storage rate of dislocations but is also affected by the flow stress superposition law, while it can be shown that $d\theta/d\sigma$ is related to the rate of dynamic recovery.

These experimental results can be qualitatively understood by applying the basic framework of Estrin[2] and Mecking and Kocks[4] with the additional consideration regarding the appropriate manner for summing the flow stress contributions from precipitation and dislocation hardening. A theoretical analysis in this framework shows that a significant change in the slope of the $\theta$-$\sigma$ plot, $d\theta/d\sigma$, accompanies the shearable/nonshearable transition. This suggests that by carefully examining the experimental data from a series of tensile tests, it is possible to determine the shearable/ nonshearable transition from the work-hardening behavior. In addition, the present work provides a semiempirical approach to interpreting a complex problem, which enables the overall mechanical response for a variety of aging conditions to be rationalized.

## LIST OF SYMBOLS

| | |
|---|---|
| $\alpha_D$ | constant relating to the storage of geometrically necessary dislocations |
| $\alpha_\perp$ | constant in the relationship between dislocation density and flow stress |
| **b** | magnitude of the Burgers vector |
| $k_1$ | dislocation storage rate term due to statistically stored dislocations |

| | |
|---|---|
| $k_2$ | dislocation storage rate term due to dynamic recovery |
| $k_D$ | dislocation storage rate term due to geometrically necessary dislocations |
| $f, f_s, f_{ns}$ | constants representing the modification of the dynamic recovery due to precipitate effects; subscripts *s* and *ns* refer to shearable and nonshearable precipitates |
| $F$ | strength of nonshearable precipitates |
| $G$ | shear modulus |
| $L$ | spacing of precipitates on the glide plane |
| $M$ | Taylor factor |
| $n$ | exponent used in flow stress addition law |
| $\varepsilon$ | total strain |
| $\varepsilon^P$ | plastic strain |
| $\rho$ | dislocation density |
| $\sigma$ | overall total flow stress of the alloy |
| $\sigma_{ss}$ | solid solution contribution to flow stress |
| $\sigma_{\text{ppt}}$ | precipitation-hardening contribution to flow stress |
| $\sigma_Y$ | yield stress |
| $\sigma_\perp$ | dislocation hardening contribution to flow stress |
| $\sigma_{\perp s}$ | saturation stress for dislocation hardening contribution |
| $T$ | line tension of the dislocation = $G\mathbf{b}^2/2$ |
| $\theta_\perp$ | work-hardening rate for dislocation hardening |
| $\theta_{\perp o}$ | initial work-hardening rate for dislocation contribution to flow stress |
| $\theta$ | overall work-hardening rate of alloy |
| $\theta_{\max}$ | overall initial work-hardening rate of alloy as defined in Fig. 3 |
| $d\theta/d\sigma$ | as defined in Fig. 3 |

## ACKNOWLEDGMENTS

This work has been supported by NSERC Canada and Alcan International. The authors also thank Hydro-Raufoss for providing the AA7030 alloy. Special thanks to S. Esmaeili for providing additional data on AA6111 and to Y. Estrin, C. Sinclair, and B. Raeisinia for useful comments on the manuscript.

## REFERENCES

1. S.J. Basinski and Z.S. Basinski: in *Dislocations in Solids,* F.R.N. Nabarro, ed., North-Holland, Amsterdam, 1979, vol. 4, pp. 261-362.
2. Y. Estrin: in *Unified Constitutive Laws of Plastic Deformation,* A.S. Krausz and K. Krausz, eds., Academic Press New York, NY, 1996, pp. 69-106.
3. U.F. Kocks: *J. Eng. Mater. Technol.,* 1976, vol. 98, pp. 76-85.
4. H. Mecking and U.F. Kocks: *Acta Metall.,* 1981, vol. 29, pp. 1865-75.
5. J.G. Sevillano: in *Materials Science and Technology,* A Comprehensive Treatment, R.W. Cahn, P. Haasen, and E.J. Kramer, eds., VCH, Weinheim, 1993, vol. 6, pp. 19-88.
6. E. Nes: *Progr. Mater. Sci.,* 1997, vol. 41 (3), pp. 129-93.
7. K. Marthinsen and E. Nes: *Mater. Sci. Eng. A,* 1997, vols. 234-236, pp. 1095-98.
8. U.F. Kocks: *Metall. Trans. A,* 1985, vol. 16A, pp. 2109-29.
9. M.Z. Butt and P. Feltham: *J. Mater. Sci.,* 1993, vol. 28, pp. 2557-76.
10. N. Ryum and J.D. Embury: *Scand. J. Metall.,* 1982, vol. 11, pp. 51-54.
11. J.G. Byrne, M.E. Fine, and A. Kelly: *Phil. Mag.,* 1961, vol. 6, pp. 1119-45.
12. E. Hornbogen and K-H.Z. Gahr: *Metallography,* 1975, vol. 8, pp. 181-202.
13. M.F. Ashby: *Phil. Mag.,* 1970, vol. 21, pp. 399-424.
14. L.M. Brown and W.M. Stobbs: *Phil. Mag.,* 1971, vol. 23, pp. 1185-99.
15. J.D. Embury: *Metall. Trans. A,* 1985, vol. 16A, pp. 2191-200.
16. A.J. Foreman and M.J. Makin: *Phil. Mag.,* 1966, vol. 14, pp. 911-24.
17. U.F. Kocks: in *Unified Constitutive Equations for Creep and Plasticity,* A.K. Miller, ed., Elsevier, London, 1987, pp. 1-88.
18. U.F. Kocks, A.S. Argon, and M.F. Ashby: in *Progress in Materials Science,* B. Chalmers, J.W. Christian, and T.B. Massalski, eds., Pergamon, Oxford, United Kingdom, 1975, vol. 19.
19. A.W. Zhu and E.A. Starke, Jr: *Acta Mater.,* 1999, vol. 47 (11), pp. 3263-69.
20. U.F. Kocks: *Proc. 5th Int. Conf. on Strength of Metals and Alloys,* P. Haasen, V. Gerold, and G. Kostorz, eds., Pergamon Press, Oxford, UK, 1979, pp. 1661-80.
21. J.T. Staley: *Aluminum Alloys: Their Physical and Mechanical Properties,* L. Arnberg, O. Lohne, E. Nes, and N. Ryum, eds., SINTEF, Trondheim, Norway, 1992, pp. 115-16.
22. M.F. Ashby: *Strengthening Methods in Crystals,* A. Kelly and R.B. Nicholson, eds., John Wiley & Sons, New York, NY, 1971, pp. 137-92.
23. L.M. Brown and R.K. Ham: *Strengthening Methods in Crystals,* A. Kelly and R.B. Nicholson, eds., John Wiley & Sons, New York, NY, 1971, pp. 12-135.
24. M. Vivas, P. Lours, C. Levaillant, A. Couret, M.J. Casanove, and A. Coujou: *Mater. Sci. Eng. A,* 1997, vol. 234–236, pp. 664-67.
25. S. Esmaeili, D.J. Lloyd, and W.J. Poole: *Acta Mater.,* 2003, vol. 51, pp. 2243-57.
26. W.F. Miao and D.E. Laughlin: *Metall. Mater. Trans. A,* 2000, vol. 31A, pp. 361-71.
27. M. Murayama, K. Hono, W.F. Miao, and D.E. Laughlin: *Metall. Mater. Trans. A,* 2001, vol. 32A, pp. 239-46.
28. D.J. Lloyd, D.R. Evans, and A.K. Gupta: *Can. Metall. Q.* 2000, vol. 39, pp. 475-82.
29. A. Perovic, D.D. Perovic, G.C. Weatherly, and D.J. Lloyd: *Scripta Mater.,* 1999, vol. 41, pp. 703-08.
30. X. Wang, W.J. Poole, S. Esmaeili, D.J. Lloyd, and J.D. Embury: *Metall. Mater. Trans. A,* in press.
31. A. Deschamps and Y. Brechet: *Acta Mater.,* 1999, vol. 47 (1), pp. 293-305.
32. W.J. Poole, J.A. Sæter, S. Skjervold, and G. Waterloo: *Metall. Mater. Trans. A,* 2000, vol. 31A, pp. 2327-38.